

## Controlled interface profile in Sm–Co/Fe exchange-spring magnets

Y. Choi<sup>a)</sup>

Materials Science Division, Argonne National Laboratory, Argonne, Illinois 60439  
and Department of Physics, University of Texas at Arlington, Arlington, Texas 76019

J. S. Jiang, J. E. Pearson, and S. D. Bader

Materials Science Division, Argonne National Laboratory, Argonne, Illinois 60439

J. J. Kavich<sup>b)</sup> and J. W. Freeland

Advanced Photon Source, Argonne National Laboratory, Argonne, Illinois 60439

J. P. Liu

Department of Physics, University of Texas at Arlington, Arlington, Texas 76019

(Received 21 June 2007; accepted 18 July 2007; published online 16 August 2007)

In exchange-spring magnets with temperature-induced interfacial intermixing, differences in the extent of diffusion of constituent elements typically lead to local compositional changes. The authors demonstrate that adding an artificially created intermixed layer in Sm–Co/Fe exchange-spring permanent magnets enhances the exchange coupling effectiveness without modifying the local composition of the Sm–Co layer. Element- and depth-resolved magnetization measurements verify that the diffusion extent of Sm and Co is similar across the interface. © 2007 American Institute of Physics. [DOI: 10.1063/1.2769755]

Nanocomposite materials offer the possibility to create unified systems from components whose properties are complementary or even mutually exclusive. Exchange-spring nanocomposite magnets<sup>1,2</sup> consist of exchange coupled nanoscale high-anisotropy (hard) and high-magnetization (soft) magnetic phases. These magnets have the potential to achieve high maximum energy product  $(BH)_{\max}$  values that define the amount of energy that a given permanent magnet can produce. In exchange-spring magnets, the  $(BH)_{\max}$  achievable is typically limited by a low switching field of the soft phase. While the intrinsic properties of the two phases play the most important role, optimization of extrinsic parameters is also important to achieve the full potential of the exchange-spring magnets. For example, interfacial conditions influence the exchange coupling that describes the magnetic interaction between the soft and hard magnetic phases. A graded interface between the two phases improves the effectiveness of the exchange coupling that consequently leads to enhanced  $(BH)_{\max}$  in Sm–Co/Fe (Refs. 3 and 4) and in CoPt/Co (Refs. 5–7) exchange-spring magnets. In comparison with an ideal interface, the graded interface leads to an increase in the anisotropy and a reduction in magnetization of the transition region, causes the soft phase to become more resistant to magnetization reversal, and thus increases the apparent coupling effectiveness between the soft and hard phases. Similarly, in exchange-spring media for magnetic recording, it was proposed that a graded interface would enhance thermal stability while reducing the writing field.<sup>8</sup> For a systematic study of these interfacial effects, tailoring interface conditions in a controllable way becomes crucial.

Sm–Co/Fe bilayers provide a simple and well-defined structure for studying fundamental aspects of exchange-spring magnets.<sup>9,10</sup> In this letter, we report the effects of add-

ing an artificially intermixed layer into Sm–Co/Fe bilayer films. In comparison with postgrowth thermal annealing,<sup>3–7</sup> the intermixed layer is created during the initial growth process and can be tailored in a more controllable way. Element-specific magnetic measurements indicate that this type of intermediate layer is less disruptive to the local Sm–Co composition near the intermediate layer.

Five Sm–Co/Fe exchange-spring bilayer samples with the sequence Cr (20 nm)/Sm–Co (20 nm)/Sm–Co–Fe ( $t_{\text{mix}}$ )/Fe (20 nm– $t_{\text{mix}}$ )/Cr (5 nm) were fabricated using magnetron sputtering.<sup>3,10</sup> For each sample, an epitaxial Sm–Co layer with a nominal composition of Sm<sub>2</sub>Co<sub>7</sub> was prepared on MgO(110) substrates covered with a 20 nm Cr(211) buffer. Subsequently, an intermediate layer consisting of alternating 0.2 nm Fe and 0.2 nm Sm–Co sublayers was deposited at 400 °C. Because of the thin individual sublayer thicknesses and the high deposition temperature, the alternately deposited sublayers most likely form an intermixed Sm–Co–Fe layer instead of retaining their individual identities. The inset of Fig. 1 shows the layer configuration of the samples. The alternating deposition of the sublayers was repeated 0, 4, 8, 12, or 25 times, resulting in an intermixed layer of thickness  $t_{\text{mix}}=0, 1.6, 3.2, 4.8, \text{ or } 10$  nm, respectively. After the intermixed layer, an Fe layer was grown at 100 °C with thickness (20 nm– $t_{\text{mix}}$ ). Finally, each sample was capped with a Cr layer. These samples are sequentially designated as M0, M16, M32, M48, and M100 throughout this letter. The main difference among the samples was the relative fraction between the intermixed Sm–Co–Fe and the Fe layers while the growth conditions of other layers were held constant. Low angle x-ray reflectivity curves using the Cu  $K\alpha$  radiation were measured on the films to check the thickness of the Sm–Co/Sm–Co–Fe/Fe layers, and the total layer thickness was within 7% of the nominal thickness for each sample.

The samples were characterized by vibrating sample magnetometry (VSM) at room temperature, and superconducting quantum interference device (SQUID) at 200 K.

<sup>a)</sup>Electronic mail: yschoi@anl.gov

<sup>b)</sup>Also at Department of Physics, University of Illinois at Chicago, Chicago, Illinois 60607.

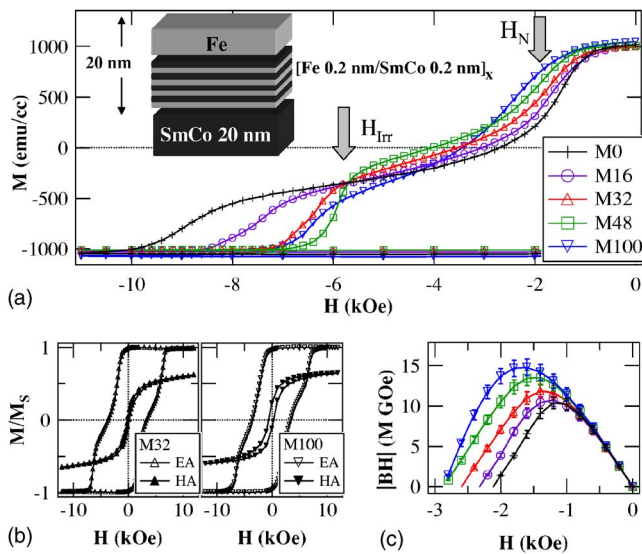


FIG. 1. (Color online) (Inset) Illustration of the layer structure. The samples have  $x$  repeating units of an Fe sublayer and a Sm–Co sublayer ( $x=0, 4, 8, 12,$  and  $25$ ). (a) VSM easy axis demagnetization curves at room temperature. (b) Easy and hard axis measurements for M32 and M100. (c) Energy product  $BH$  as a function of demagnetizing field  $H$ .

Element- and depth-sensitive demagnetization curves were measured by utilizing  $x$ -ray resonant magnetic scattering (XRMS) magnetometry<sup>11–15</sup> on M32 and M100 at 200 K. The XRMS measurements were performed at beamline 4ID-C of the Advanced Photon Source at Argonne National Laboratory.<sup>16</sup> The XRMS measurements were made at the Fe  $L_3$ , Co  $L_3$ , and Sm  $M_5$  absorption edges to probe the Fe, Co, and Sm atoms, respectively. Element-specific XRMS demagnetization curves were obtained by collecting the asymmetry ratio as a function of external magnetic field  $H$  at a fixed  $x$ -ray energy and specular angle ( $\sim 12^\circ$ ). The asymmetry ratio is defined as  $(I^+ - I^-)/(I^+ + I^-)$ , where  $I^{\pm}$  are the scattered intensities for the two opposite circular polarizations of the incoming  $x$  rays. In general, the  $x$ -ray attenuation effect is significant at low incident angles. Taking advantage of this, XRMS magnetometry measurements can provide depth-sensitive magnetic characterization, in addition to element specificity. The  $x$ -ray energy and incident angle conditions were predetermined, based on our previous work,<sup>17</sup> in order to keep the same  $x$ -ray penetration depths for the Sm and Co measurements.

The easy axis VSM demagnetization curves are shown in Fig. 1(a). For each curve, two switching fields are distinguishable. The nucleation field  $H_N$  in the low field range marks the reversible magnetization switching in the Fe layer, and the switching field  $H_{irr}$  in the high field range is due to the irreversible switching of the Sm–Co layer. As the intermixed layer thickness increases,  $H_N$  increases while  $H_{irr}$  decreases. This trend continues from M0 to M48. For M100, the  $H_N$  is higher than that of M48, but  $H_{irr}$  does not decrease anymore. Easy and hard axis measurements for M32 and M100 are shown in Fig. 1(b). Up to M48, the hard axis measurements do not show hysteresis effects, indicating that those samples have well-defined uniaxial anisotropy. However, for M100, the hard axis hysteresis loop encloses an area. This result suggests that at least up to M48, the uniaxial anisotropy direction of the intermixed layer follows that of the Sm–Co layer below. It is conceivable that the intermixed layer of 10 nm is thick enough to have some regions with the

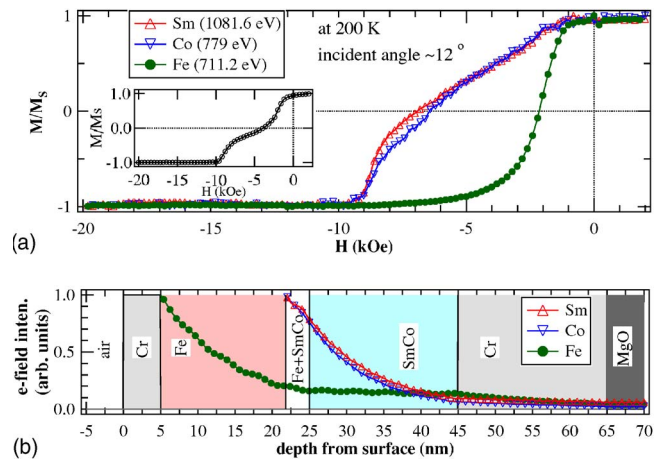


FIG. 2. (Color online) From M32 [Fe (16.8 nm)/mix (3.2 nm)/Sm–Co (20 nm)]. (a) Measured Sm-, Co-, and Fe-specific XRMS demagnetization curves. The inset shows the SQUID result. (b) Calculated electric field intensity variations at the Fe  $L_3$ , Co  $L_3$ , and Sm  $M_5$  absorption energies.

anisotropy direction deviating from that of the Sm–Co layer below.

Based on the demagnetization curves in Fig. 1(a), the corresponding energy product values  $(BH) = |(4\pi\mathbf{M} + \mathbf{H}) \cdot \mathbf{H}|$  are calculated as shown in Fig. 1(c). As the intermixed layer thickness increases, the  $(BH)_{max}$  value gradually increases due to the increased  $H_N$ . The increased  $H_N$  stems from an increase in exchange coupling effectiveness, as similarly observed in exchange-spring magnets after the thermal annealing process.<sup>3,5–7</sup> The interdiffusion at the interfaces leads to the formation of a region with intermediate anisotropy values, which improves the effectiveness of exchange coupling. However, this process entails magnetic softening of the hard phase and changing the local composition of the hard phase. In Sm–Co/Fe films, different extents of Sm and Co diffusions across the interface have been observed by electron energy loss spectroscopy<sup>3,4</sup> and by element-specific demagnetization curves.<sup>17,18</sup> In these works, prominently higher Co diffusion into the Fe layer has been observed. For permanent magnets for high temperature applications, the difference in the extent of diffusion may lead to hard phase compositional changes in a less controllable way. This difference in the extent of diffusion may not be avoided entirely. However, the extent is expected to be reduced in our present samples with an intermixed layer since the composition gradients across the Sm–Co/intermixed interface are less abrupt. In order to verify this, we performed depth- and element-sensitive XRMS magnetometry measurements.

The XRMS results from M32 and M100 are shown in Figs. 2(a) and 3(a), respectively. In order to estimate the  $x$ -ray penetration depth (thus the probed volume) for each demagnetization curve measurement, we calculated  $x$ -ray electric field intensity profiles<sup>19</sup> for the experimental conditions used [Figs. 2(b) and 3(b)]. For clarity, the electric field intensity profile for the Fe measurements was normalized to the intensity at the top of the Fe layer, and the profiles for the Sm and Co measurements were normalized to the respective intensities at the bottom of the Fe layer. In Fig. 2(a), the Sm and Co XRMS curves of M32 show a gradual change between  $-1$  and  $-8$  kOe before the abrupt reversal near  $-10$  kOe. The reversal in this bilayer is expected to initiate from the top Fe surface and move gradually toward the

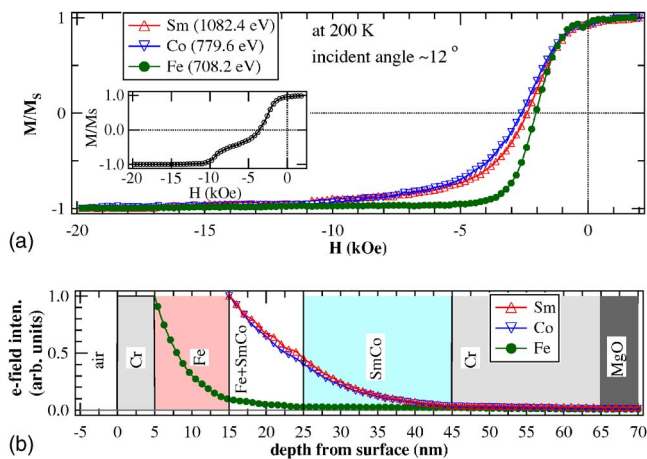


FIG. 3. (Color online) From M100 [Fe (10 nm)/mix (10 nm)/Sm–Co (20 nm)]. (a) Measured Sm-, Co-, and Fe-specific XRMS demagnetization curves. The inset shows the SQUID result. (b) Calculated electric field intensity variations.

Sm–Co layer. The observed gradual XRMS magnetization change is due to the intermixed layer and the regions near it, while the abrupt reversal is due to the bottom Sm–Co layer. The volume-averaged SQUID demagnetization curve for this bilayer is shown as inset of Fig. 2, where the irreversible switching occurs near  $-10$  kOe. On the other hand, M100 has a thicker intermixed layer, and the Sm and Co XRMS demagnetization curves are dominated by the signals from the intermixed layer, as shown in Fig. 3(a). The Sm and Co demagnetization curves have slowly decreasing tails until  $-10$  kOe, where the irreversible switching was observed in SQUID measurement (inset of Fig. 3).

In the previous element-specific magnetism studies on Sm–Co/Fe bilayers with temperature-induced interfacial intermixing, the Sm- and Co-demagnetization curves were different due to different extents of Sm and Co diffusions.<sup>17,18</sup> Such a difference in Sm and Co diffusions would necessarily mean a modification of the local composition and hence a reduced anisotropy of the Sm–Co hard layer. The situation is quite different in the present samples. The calculated x-ray intensity profiles in Figs. 2(b) and 3(b) show that the intensity variations for the Sm and Co measurements are almost the same, and this result confirms that almost the same volume was probed in the Sm and Co XRMS measurements. Figure 2(a) shows that the Sm and Co XRMS demagnetization curves are similar to each other, and Fig. 3(a) shows the same trend. The close similarity between the Sm and Co demagnetization curves indicates that the extent of Sm and Co diffusions is similar and that the local Sm–Co composition is not changed across the Sm–Co/Fe interface in the present samples.

Our work demonstrates that interfacial structures with a controlled interfacial profile can be fabricated by alternating sublayer deposition. The local chemical composition across the interfacial region may be changed by varying the thickness ratio between the Sm–Co and Fe sublayers during the fabrication of an intermixed layer. This would lead to corresponding variations in the profile of the magnetic parameters across the interface. This approach opens up the possibility to fabricate arbitrary interface profiles in order to experimentally investigate the optimal anisotropy profile across the soft and hard bilayer interfaces for improved effective exchange coupling, and thus increased  $(BH)_{\max}$  value, as theoretically studied in Refs. 8 and 20.

This work was supported by ONR/MURI under Grant No. M00014-05-1-0497. Work at Argonne National Laboratory was supported by U.S. Department of Energy, Office of Science, under Contract No. DE-AC02-06CH11357.

- <sup>1</sup>E. F. Kneller and R. Hawig, IEEE Trans. Magn. **27**, 3588 (1991).
- <sup>2</sup>R. Skomski and J. M. D. Coey, Phys. Rev. B **48**, 15812 (1993).
- <sup>3</sup>J. S. Jiang, J. E. Pearson, Z. Y. Liu, B. Kabius, S. Trasobares, D. J. Miller, S. D. Bader, D. R. Lee, D. Haskell, G. Srajer, and J. P. Liu, Appl. Phys. Lett. **85**, 5293 (2004).
- <sup>4</sup>J. Zhang, Y. K. Takahashi, R. Gopalan, and K. Hono, Appl. Phys. Lett. **86**, 122509 (2005).
- <sup>5</sup>J. Kim, K. Barmak, M. De Graef, L. H. Lewis, and D. C. Crew, J. Appl. Phys. **87**, 6140 (2000).
- <sup>6</sup>D. C. Crew, J. Kim, L. H. Lewis, and K. Barmak, J. Magn. Magn. Mater. **233**, 257 (2001).
- <sup>7</sup>L. H. Lewis, J. Kim, K. Barmak, and D. C. Crew, J. Phys. D **37**, 2638 (2004).
- <sup>8</sup>D. Suess, Appl. Phys. Lett. **89**, 113105 (2006).
- <sup>9</sup>K. Mibu, T. Nagahama, T. Shinjo, and T. Ono, Phys. Rev. B **58**, 6442 (1998).
- <sup>10</sup>E. E. Fullerton, J. S. Jiang, M. Grimsditch, C. H. Sowers, and S. D. Bader, Phys. Rev. B **58**, 12193 (1998).
- <sup>11</sup>C. Kao, J. B. Hastings, E. D. Johnson, D. P. Siddons, G. C. Smith, and G. A. Prinz, Phys. Rev. Lett. **65**, 373 (1990).
- <sup>12</sup>J. W. Freeland, K. Bussmann, P. Lubitz, Y. U. Idzerda, and C. C. Cao, Appl. Phys. Lett. **73**, 2206 (1998).
- <sup>13</sup>Y. Choi, D. R. Lee, J. W. Freeland, G. Srajer, and V. Metlushko, Appl. Phys. Lett. **88**, 112502 (2006).
- <sup>14</sup>E. Negusse, A. Lussier, J. Dvorak, Y. U. Idzerda, S. R. Shinde, Y. Nagamine, S. Furukawa, K. Tsunekawa, and D. D. Djayaprawira, Appl. Phys. Lett. **90**, 092502 (2007).
- <sup>15</sup>S. Roy, C. Sanchez-Hanke, S. Park, M. R. Fitzsimmons, Y. J. Tang, J. I. Hong, D. J. Smith, B. J. Taylor, X. Liu, M. B. Maple, A. E. Berkowitz, C.-C. Kao, and S. K. Sinha, Phys. Rev. B **75**, 014442 (2007).
- <sup>16</sup>J. W. Freeland, J. C. Lang, G. Srajer, R. Winarski, D. Shu, and D. M. Mills, Rev. Sci. Instrum. **73**, 1408 (2002).
- <sup>17</sup>Y. Choi, J. S. Jiang, Y. Ding, R. A. Rosenberg, J. E. Pearson, S. D. Bader, A. Zambano, M. Murakami, I. Takeuchi, Z. L. Wang, and J. P. Liu, Phys. Rev. B **75**, 104432 (2007).
- <sup>18</sup>M.-H. Yu, J. Hattrick-Simpers, I. Takeuchi, J. Li, Z. L. Wang, S. E. Lofland, S. Tyagi, J. W. Freeland, D. Giubertoni, M. Bersani, and M. Anderle, J. Appl. Phys. **98**, 063908 (2005).
- <sup>19</sup>L. G. Parratt, Phys. Rev. **95**, 359 (1954); D. K. G. de Boer, Phys. Rev. B **44**, 498 (1991).
- <sup>20</sup>D. C. Crew, J. Appl. Phys. **91**, 7212 (2002).